CONTRIBUTION TO SYNTHESIS OF ZnO NANOPARTICLES BY UV IRRADIATION-ASSISTED PRECIPITATION

PRAUS Petr, TOKARSKÝ Jonáš, SVOBODA Ladislav

VSB - Technical University of Ostrava, Ostrava, Czech Republic, EU, petr.praus@vsb.cz

Abstract

This work is a contribution to our previous research in which we dealt with the influence of different preparation methods on fundamental properties of ZnO nanoparticles. Our current research was focused on the formation of oxygen vacancies in ZnO nanoparticles, especially by the UV radiation-assisted precipitation. The models of ZnO vacant structures were built in the Materials Studio Environment. The modelling results showed that under UV irradiation the higher amount of large oxygen vacancies was created and resulting strain in the ZnO structure likely lead to disintegration of the ZnO nanoparticles into the smaller ones, i.e. from the mean size from 25 nm to 15 nm, as observed by transmission electron microscopy (TEM).The concentrations of dissolved oxygen in ZnO aqueous nanodispersions were measured during their synthesis. The significant decrease of the oxygen concentration during UV irradiation indicated that hydroxyl radicals were generated and the oxygen vacancies were formed by photocorrosion of the already precipitated ZnO nanoparticles.

Keywords: ZnO nanoparticles, oxygen vacancies, UV irradiation, precipitation, molecular modelling.

1. INTRODUCTION

Zinc oxide crystallizes in the hexagonal wurtzite and cubic zinc blende forms having structure defects like oxygen vacancies and zinc interstitials [1]. This semiconductor has many unique and fascinating properties, such as superior mechanical toughness [2], good transparency, high electron mobility and strong room-temperature luminescence [3]. ZnO nanostructures can be synthesized into a variety of morphologies, including nanowires, nanorods, tetrapods, nanobelts, nanoflowers and nanoparticles [4]. Many methods have been described for the synthesis of ZnO nanomaterials, such as laser ablation [5], hydrothermal methods [6], electrochemical depositions [7], and sol-gel method [8] and even radiolytic synthesis [9,10].

In our previous work [11] we showed that the different ZnO syntheses can produce nanostructures with the different number of structure defects, such as the energy of band gap, photoluminescence intensity, particle sizes, and photocatalytic activity. Oxygen vacancies concentrated on surfaces of ZnO nanoparticles (NPs) are able to trap electrons and thus decrease their photocatalytic activity. This effect was mainly observed in case of ZnO prepared by the UV irradiation assisted precipitation.

The aim of this research was to study the ZnO precipitation under UV irradiation, especially formation of oxygen vacancies. For this purpose, the molecular modelling of ZnO structures was applied. The size of ZnO NPs was estimated from transmission electron microscopy (TEM) images. In order to find formation mechanisms of the oxygen vacancies, the concentration of dissolved oxygen in ZnO aqueous dispersions was measured during the precipitation.

2. EXPERIMENTAL

2.1. Material and chemicals

The used zinc acetate dihydrate and sodium hydroxide (both from Lachema, Czech Republic) were of analytical reagent grade. Water deionised by reverse osmosis (Aqua Osmotic, Czech Republic) was used for the preparation of all solutions.

2.2. Molecular modelling

The molecular modelling of the ZnO oxygen vacancies was performed in the Materials Studio 4.2 modelling environment in the Forcite module using Universal force field [12]. Based on the results of XRPD, the unit cell of hexagonal ZnO having the lattice parameters a = 3.24927 Å, b = 3.24927 Å, c = 5.20544 Å, α = 90°, β = 90°, γ = 120° was taken from the Materials Studio library. All models were prepared as 8×8×8 supercell ($Zn_{1024}O_{1024}$) with the lattice parameters a = 25.9942 Å, b = 25.9942 Å, c = 41.6435 Å, α = 90°, β = 90°, γ = 120°, under the periodic boundary conditions. All atomic charges were calculated using the charge equilibration (QEq) method [13].

2.3. Transmission electron microscopy

Transmission electron microscopy with high resolution images of the ZnO NPs were examined by a JEM 220FS microscope (Jeol, Japan) operating at 200 kV. The NPs were dispersed in ethanol and deposited on a TEM grid with carbon holey support film using an ultrasonic sprayer.

2.4. Measuring dissolved oxygen

A multi-parameter meter (Multi 3420, WTW GmbH, Germany) equipped with a dissolved oxygen probe was used for dissolved oxygen measurements. During the measurements ZnO aqueous nanodispersions were stirred.

2.5. Preparation of nanoparticles

Into the stirred solution of 60 ml 3.3 mmol·l^{-1} zinc acetate was added dropwise 40 ml 15 mmol·l^{-1} NaOH (the flow rate was of about 0.67 ml·min^{-1}). The ratio of zinc acetate : sodium hydroxide was 1 : 3. The resulting dispersions were filtered and the filter cakes were subsequently annealed at 350 °C for 2 hours. The precipitation assisted by UV irradiation was performed in the presence of a medium-pressure Hg UV lamp with the maximum emission intensity at the wavelength of 254 nm.

3. RESULTS AND DISCUSSION

3.1. Preparation and characterization of ZnO nanoparticles

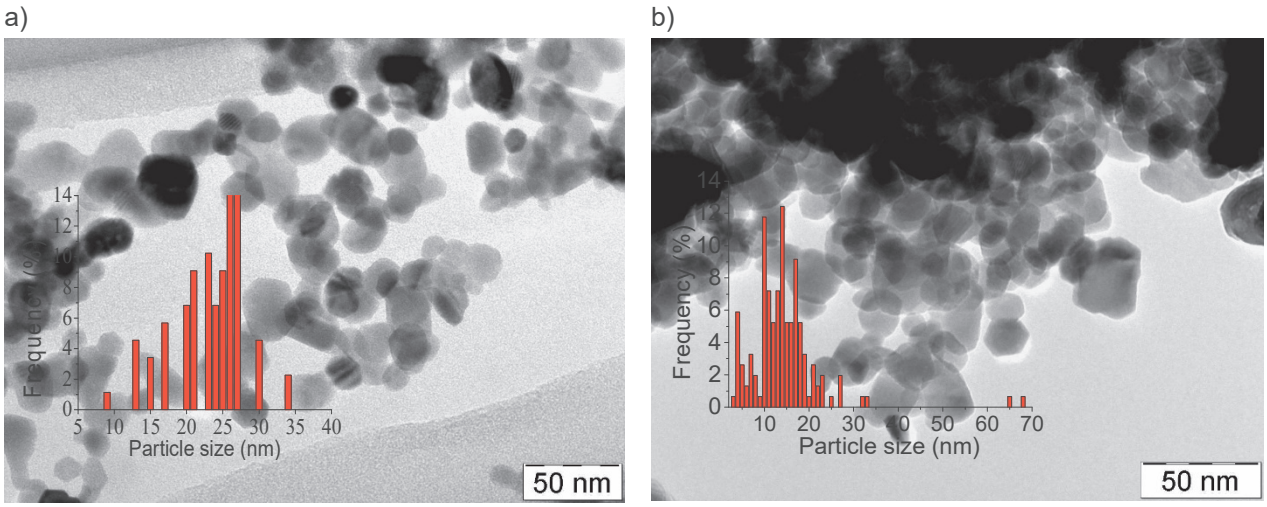

Fig. 1 TEM images of ZnO nanoparticles. (a) ZnO[1] nanoparticles, (b) ZnO[2] nanoparticles. Size distribution histograms were placed as insets

The ZnO NPs were prepared by a) the precipitation of zinc acetate with sodium hydroxide followed by thermal annealing at 350 °C and b) by the same manner but the precipitation was performed under UV irradiation. The

resulting nanoparticles were characterized by XRPD, the photoluminescence and diffuse reflectance spectroscopy of which results confirmed the observations published in our previous paper [11].

Besides, the obtained ZnO NPs were examined by TEM. The TEM image analysis (**Fig. 1**) showed that the precipitation without UV irradiation formed the larger ZnO nanoparticles (ZnO^1) that the same precipitation with UV irradiation (ZnO^2). The mean size of ZnO^1 nanoparticles was about 25 nm while the mean size of ZnO^2 nanoparticles was about 15 nm.

Our previous results of spectral analyses and photocatalytic experiments [11] demonstrated that the synthesis with UV irradiation produced the ZnO NPs with the higher number of oxygen vacancies. In order to understand the formation of these oxygen vacancies the vacant ZnO structures were modelled in the Material Studio modelling environment.

3.2. Molecular modelling

Six models of the ZnO hexagonal structure having 24 oxygen atoms vacancies were prepared. The models 1000_a, 1000_b and 1000_c have 24 oxygen vacancies equally distributed in the volume, but the positions of vacancies in each model were different. On the contrary, in the models 1000_d, 1000_e, and 1000_f all 24 oxygen vacancies were located together. Three oxygen rows were removed in each model: two horizontally and one below (**Fig. 2a**), three horizontally (**Fig. 2b**), and three vertically (**Fig. 2c**).

The geometry optimizations of all models were carried out in the Materials Studio modelling environment in Forcite module using Universal force field [12]. A smart algorithm with 50,000 iteration steps was used. The convergence thresholds for the maximum energy, force, and displacement changes were $2 \cdot 10^{-5}$ kJ·mol^{-1}, $1 \cdot 10^{-3}$ kJ·mol^{-1}·Å^{-1}, and $1 \cdot 10^{-5}$ Å, respectively.

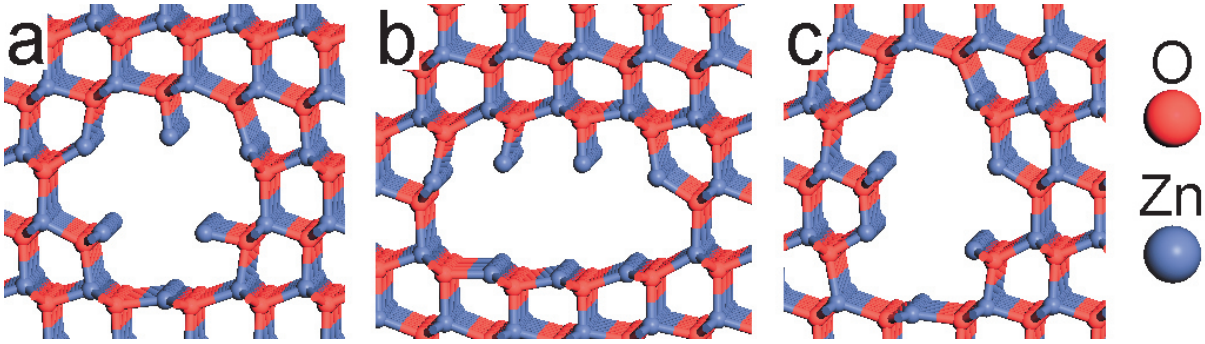

Fig. 2 Oxygen vacancies are located together in models (a) 1000_d, (b) 1000_e, and (c) 1000_f

The optimized models were analyzed using the Bond distribution tool in the Forcite module (bin width 0.01 Å). **Fig. 3** shows the comparison of bond lengths distributions for models having vacancies equally distributed throughout the volume (1000_a, 1000_b, 1000_c) and the models having the same number of vacancies located together (1000_d, 1000_e, 1000_f). It is evident that range of lengths in the models 1000_d, 1000_e, and 1000_f is broader than in the other models. It can be concluded that vacancies located together influenced the bond lengths more than the oxygen vacancies distributed equally.

Diffraction data calculated from the optimized models in the Materials Studio/Reflex module under the same conditions as the real XRPD analysis was performed [11] allow us to find the similarity between the model and measured diffractograms. The ratios of intensities of various *hkl* reflections were used as the similarity descriptors. The total similarity of the model and real diffractograms of ZnO^1 and ZnO^2 NPs was quantified as the sum of differences (ΣΔ) between the ratios. In an ideal case, the diffractograms would be identical if ΣΔ would be equal to zero. Two models having the vacancies located together (1000_d and 1000_f) exhibited the best similarity with the ZnO^2 nanoparticles. In addition, based on the ΣΔ values it was concluded that the ZnO^2 nanoparticles contained the higher amount of the oxygen vacancies than the ZnO^1 ones.

In these models the joined oxygen vacancies likely caused significant strain and distortion in the ZnO[1] NPs which led to their disintegration into smaller ZnO[2] ones as demonstrated by their mean sizes (**Fig. 1**).

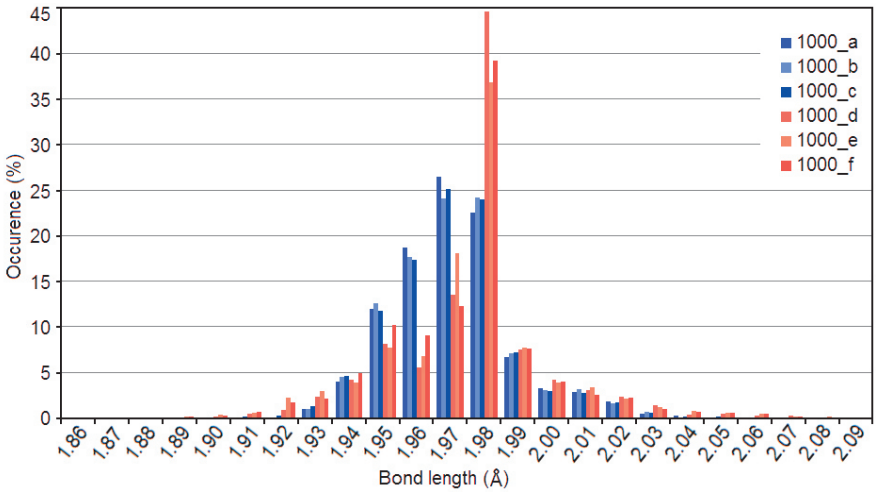

Fig. 3 Difference between distributions of bond lengths in models having oxygen vacancies equally distributed in volume (1000_a, 1000_b, 1000_c) and models having oxygen vacancies located together (100_d, 1000_e, 1000_f)

3.3. Determination of dissolved oxygen

The oxygen vacancy formation was investigated by the determination of oxygen dissolved in the aqueous ZnO dispersions during the precipitation (**Fig. 4**). When ZnO[1] was precipitated the concentration of oxygen was nearly constant but when UV irradiation was applied the concentration significantly decreased. The explanation of this effect is that the originating ZnO nuclei absorbed UV photons and generated electron and holes. Consequently, these electrons reacted with dissolved oxygen forming hydroxyl radicals by mechanisms published elsewhere [14,15].

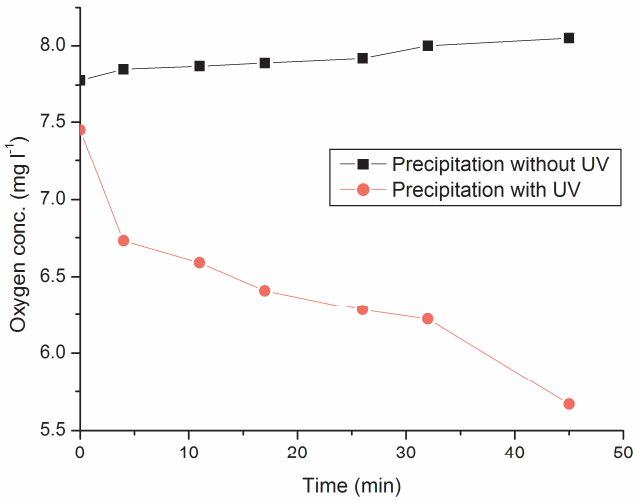

Fig. 4 Concentrations of dissolved oxygen during the precipitation of ZnO

The hydroxyl radicals are known to have strong oxidation properties characterized by the high standard redox potentials of 2.4-2.6 V. The reaction of the hydroxide radicals with The ZnO surface oxygen atoms can be assumed as

$$ZnO + OH^{\bullet} \rightarrow Zn^{2+} + O^{\bullet -} + OH^{-} \quad (1)$$

forming the oxygen vacancies on the ZnO NPs surface and $O^{\bullet}$ radicals [14]. This reaction demonstrates photocorrosion of the previously precipitated NPs, which was not detrimental for them but led to the enhancement of their photoluminescence [11] and the formation of the smaller ZnO^2 NPs.

Besides, the hydroxyl radicals are supposed to oxidize zinc acetate as follows

$$(CH_3COO)_2Zn + 16\ OH^{\bullet} \rightarrow 4\ CO_2 + 10\ H_2O + Zn(OH)_2 \quad (2)$$

By this reaction additional $Zn(OH)_2$ molecules were produced which likely enhanced the ZnO precipitation. The resulting supersaturation of $Zn(OH)_2$ could also lead to formation of the smaller ZnO NPs. Such complex mechanism encompassing the photocorrosion and fast nanoparticles growth due to the supersaturation could be a topic for another research.

4. CONCLUSION

In this work, the formation of oxygen vacancies in the ZnO NPs synthetized by the precipitation with and without UV irradiation was investigated. The molecular modelling revealed that the ZnO NPs synthetized by the UV irradiation-assisted precipitation contained the higher amount of large oxygen vacancies. The strain caused by the different bond lengths of such large vacancies was likely the reason for the formation of smaller ZnO NPs with the mean size of 15 nm in comparison with the larger sized NPs of 25 nm prepared by the conventional precipitation.

The determination of dissolved oxygen during the precipitation indicated that the large oxygen vacancies were created by the photocorrosion caused by reactions of the hydroxyl radicals with oxygen atoms on the ZnO NPs surface. It is obvious that the photocorrosion was not detrimental for the ZnO NPs but decreased their size.

Besides common thermal treatment under different atmospheres [16], the controlled photocorrosion could be a useful method for the preparation of small luminescent ZnO NPS for various applications. In addition, application of such controlled photocorrosion on other oxide NPs could be tested in the future.

ACKNOWLEDGEMENTS

The authors thank the "National Feasibility Program I", the project LO1208 "TEWEP" from the Ministry of Education, Youth and Sports of the Czech Republic, the European Regional Development Fund in the IT4Innovations Centre of Excellence (project CZ.1.05/1.1.00/02.0070) and the project SP 2015/76 from VŠB-TU Ostrava for their financial support.

REFERENCES

[1] WAGNER P., HELBIG R. Halleffekt und anisotropie der beweglichkeit der elektronen in ZnO. Journal of Physics and Chemistry of Solids, Vol. 35, No. 3, 1974, pp. 327-335.

[2] YONENAGA I. Thermo-mechanical stability of wide-bandgap semiconductors: high temperature hardness of SiC, AlN, GaN, ZnO and ZnSe. Physica B: Condensed Matter, Vol. 308, No. 1, 2001, pp. 1150-1152.

[3] KUMAR S. S., VENKATESWARLU P., RAO R. V., RAO N. G., Synthesis, characterization and optical properties of zinc oxide nanoparticles. International Nano Letters, Vol. 3, No. 1, 2013, pp. 1-6.

[4] WANG R. CH., TSAI CH. CH. Efficient synthesis of ZnO nanoparticles, nanowalls, and nanowires by thermal annealing of zinc acetate at a low temperature. Applied Physics A, Vol. 94, No. 2, 2009, pp. 241-245.

[5] RYU Y. R., LEE T. S., WHITE H. W. Properties of arsenic-doped p-type ZnO grown by hybrid beam deposition. Applied Physics Letters, Vol. 83, 2003, p. 87.

[6] NI Y. H., WEI X.W., HONG J. M., YE Y. Hydrothermal preparation and optical properties of ZnO nanorods. Materials Science and Engineering: B, Vol. 121, No. 1, 2005, pp. 42-47.

[7] CHANG S.S., YOON S.O., PARK H. J., SAKAI A. Luminescence properties of Zn nanowires prepared by electrochemical etching. Materials Letters, Vol. 53, No. 6, 2002, pp. 432-436.

[8] RISTIĆ M., MUSIĆ S., IVANDA M., POPOVIĆ S. Sol-gel synthesis and characterization of nanocrystalline ZnO powders. Journal of Alloys and Compounds, Vol. 397, No. 1, 2005, pp. 1-4.

[9] RATH M. C., SUNITHA Y., GHOSH H. N., SARKAR S. K., MUKHERJEE T. Investigation of the dynamics of radiolytic formation of ZnO nanostructured materials by pulse radiolysis. Radiation Physics and Chemistry, Vol. 78, No. 2, 2009,pp. 77-80.

[10] ČUBA V., GBUR T., MÚČKA V., KUČERKOVÁ R., POSPÍŠIL M., JAKUBEC I. Properties of ZnO nanocrystals prepared by radiation method. Radiation Physics and Chemistry, Vol. 79, No. 1, 2010, pp. 27-32.

[11] RELI M., EDELMANNOVÁ M., ŠIHOR M., PRAUS P., SVOBODA L., MAMULOVÁ-KUTLÁKOVÁ K.,OTOUPALÍKOVÁ H., ČAPEK L., HOSPODKOVÁ A., OBALOVÁ L., KOČÍ K. Photocatalytic H_2 generation from aqueous ammonia solution using ZnO photocatalysts prepared by different methods. International Journal of Hydrogen Energy, Vol. 40, No. 27, 2015, pp. 8530-8538.

[12] RAPPÉ A. K., CASEWIT C. J., COLWELL K. S., GODDARD III. W. A., SKIFF W. M. UFF, a full periodic table force field for molecular mechanics and molecular dynamics simulations. Journal of the American Chemical Society, Vol. 114, No. 25, 1992, pp. 10024-10035.

[13] RAPPÉ A. K., GODDARD III. W. A. Charge equilibration for molecular dynamics simulations. The Journal of Physical Chemistry, Vol. 95, No. 8, 1991, pp. 3358-3363.

[14] BUXTON G. V., GREENSTOCK C. L., HELMAN W. P., ROSS A. B. Journal of Physical and Chemical Reference Data. Critical Review of Rate Constants for Reactions of Hydrated Electrons, Hydrogen Atoms and Hydroxyl Radicals ($^{\bullet}OH/^{\bullet}O^-$) in Aqueous Solutions, Vol. 17, No. 2, 1988, pp. 513-533.

[15] FENG W., JING L., ZHANG P., NANSHENG D. Photochemical formation of hydroxyl radical catalysed by montmorillonite. Chemosphere, Vol. 72, No. 4, 2008, pp. 407-413.

[16] DROUILLY CH., KRAFT J.M., AVERSENG F., CASALE S., BAZER-BACHI D., CHIZALLET C., LECOCQ V., VEZIN H., LAURON-PERNOT H., COSTENTIN G. ZnO Oxygen Vacancies Formation and Filling Followed by in Situ Photoluminescence and in Situ EPR. The Journal of Physical Chemistry, Vol. 116, No. 40, 2012, pp. 21297-21307.